CHAPTER 6

Evidence of broad tricritical range for the smectic-*A* to smectic-*C* phase transition

6.1. Introduction

Liquid crystals formed by bent-shaped molecules have been a subject of intense experimental and theoretical investigations due to their unique properties and potential applications in the field of fast switching displays [1-5]. In spite of usual bent-shaped molecules, delicate modifications in molecular structure may yield calamitic like polymorphisms involving smectic-*C* (Sm-*C*), smectic-*A* (Sm-*A*) and even nematic (*N*) phases [6-10]. However, the interest on molecular behavior and appearance of different exceptional mesophases in pure bent-core liquid crystals, binary mixtures composed of bent-shaped and rod-like molecules have shown various interesting phenomena [11–13] and novel phase transitions [3,14], which brought them at the center of scientific interest and stimulates considerable research efforts regarding formulation and characterization of noble liquid crystalline mixtures. The effect of mixing on the mesophase sequence and transitional behavior in such doped system is of unparalleled advantage for obtaining a deeper understanding of the unresolved issues regarding transitional phenomena in soft matter systems.

Over the past few decades, the nature of the smectic-*A*–smectic-*C* (Sm-*A*–Sm-*C*) transition has been a topic of great interest in an effort to determine the order of the transition and the universality class to which it belongs [15-29]. Despite considerable progress, the critical characteristics and universality class of the Sm-*A*–Sm-*C* phase transition remains only partially unveiled and till now has been treated as a controversial issue in the field of equilibrium statistical mechanics of soft condensed matter [17,22-29].

In the previous chapter (chapter 5), a high-resolution temperature scanning technique was successfully used in determining the optical birefringence (Δn) precisely throughout the mesomorphic range and discusses the possibility of crossover behavior from tricritical to 3D-*XY* critical nature near the Sm-*A*–Sm-*C* transition in a binary system belonging to the same homologous series of phenyl pyrimidine compounds [30,31]. It has been shown

that the character of the Sm-*A*–Sm-*C* transition is really critical over the reduced temperature range 3×10^{-3}, estimated in the range of 2 K from the transition. The non-universal behavior of this transition with either very weak first-order or second-order transitions was explained on the basis of the Sm-*A* temperature range linked with the Sm-*A*–Sm-*C* phase transition. It should be noted that, these binary mixtures of rod-like compounds was found to demonstrate a variation of the Sm-*A* phase range from 11 K to 19 K. However, the extrapolation of the linear fit yields a crossover from second order to first order nature at the Sm-*A* range ~10.5 K. Therefore, it is of great interest to investigate how does further reduction of the Sm-*A* range influences the transitional behavior of the Sm-*A*–Sm-*C* phase transition. On the other hand, it is also interesting to characterize the critical fluctuations near the Sm-*A*–Sm-*C* transition for the mixtures of compounds having complex and varied molecular structure rather than the mixtures of homologous compounds.

The present chapter is mainly dedicated to focus on an extensive optical investigation in a binary system comprising of a laterally methyl substituted hockey stick-shaped compound (H-22.5) and a calamitic compound (7OCB). The temperature-dependent optical birefringence (Δn) value has been measured from the high-resolution temperature scanning technique and hence employed to take a deeper insight into the critical behavior associated with the Sm-*A*–Sm-*C* phase transition. The values of the effective critical exponent α' have been explored with the variation of Sm-*A* temperature range and the observed outcomes are discussed in light of the crossover behavior. However, an attempt has also been made to test the plausibility of tricriticality nature of the Sm-*A*–Sm-*C* phase transition by modifying the renormalization group expression with additional correction terms. Interestingly, in spite of the steep phase boundary, no sign of the Fisher renormalization of the critical exponent has been found, even for the tricritical mixtures.

6.2. Materials

The hockey stick-shaped compound, 4-(3-n-decyloxy-2-methyl-phenyliminomethyl) phenyl 4-n-dodecyloxy cinnamate (H-22.5) was obtained from the Institute of Physical Chemistry, Martin Luther University, Halle, Germany and the compound 4-cyano-4′-heptyloxybiphenyl (7OCB) was purchased from E. Merck, UK (having a purity higher than 99.9%) and were used to prepare the mixtures without further purification. The structural formulae and transition scheme for both the pure compounds are given in Fig. 6.1.

Compound 1:

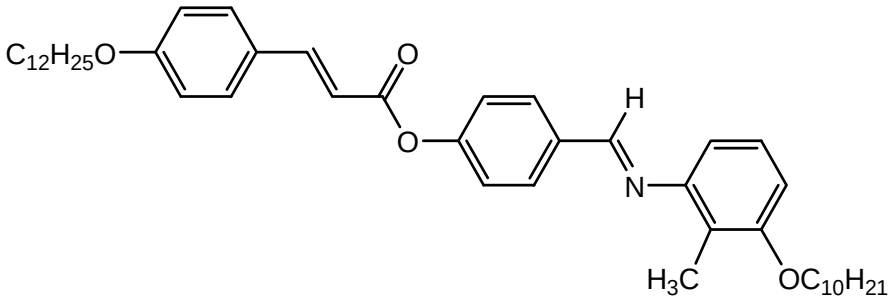

Cr (347.2 K) **Sm-*C*$_a$** (374.4 K) **Sm-*C*$_s$** (382.8 K) ***N*** (383.1 K) ***I***

Compound 2:

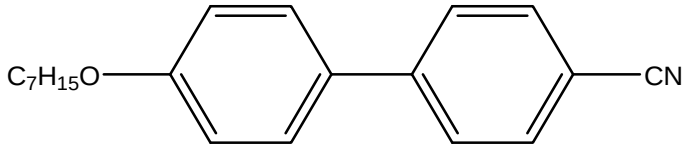

Cr (327 K) ***N*** (347 K) ***I***

Figure. 6.1. Chemical structure and phase behavior of the hockey-stick-shaped compound (Compound 1: H-22.5) and the rod-like compound (Compound 2: 7OCB).

Nine different mixtures with molar concentrations of x_{7OCB} = 0.211, 0.2, 0.184, 0.174, 0.167, 0.158, 0.15, 0.1 and 0.05 have been prepared by adding small amounts of the rod-like compound (7OCB) into the host hockey stick-shaped mesogen. The phase transition temperatures were determined from polarizing optical microscopy and optical transmission technique.

6.3. Texture observation

The optical textures of different mesophases of the studied mixtures were observed under a polarizing optical microscope (BANBROS) equipped with INSTEC HCS302 hot stage, controlled by INSTEC mK1000 thermo system. Three distinct mesophases have been detected by polarized light optical microscopy for all of the investigated mixtures, out of them optical textures for the mixture x_{7OCB} = 0.184 is presented in Fig. 6.2. The high-temperature mesophase behaves like the conventional Sm-*A* phase, characterized by a typical fan-shaped texture in planar alignment cell (Fig. 6.2(a)). The homeotropically aligned areas are found optically isotropic and appears completely dark between the crossed polarizers (Fig. 6.2(d)). Such an appearance indicates the presence of the Sm-*A* phase. On further cooling in planar oriented samples, a broken fan-like texture emerges with a significant change in the birefringence near the phase transition (Fig. 6.2(b)). However, the color change from green to yellow indicates an increase in the effective birefringence of the sample. On the other hand, the appearance of schlieren texture has also been seen in homeotropic alignment which indicates a transition to a new optically biaxial mesophase (Fig. 6.2(e)). These textural features are in general a gesture for Sm-C_s phases [6] where the direction of the molecular tilt is the same in adjacent smectic layers. Similar types of textures were often observed experimentally in pure hockey stick-shaped compounds [6,8]. The transition to the third lower temperature mesophase has been ascertained by a clear change in the optical textures. On cooling the sample, the broken fan-shaped texture of the Sm-C_s phase modified with irregular stripes [Fig. 6.2(c)], arises sharply across the fans and this optical feature sustains further to some definite range of temperature below the transition. This is the indication of the transition to an anticlinic Sm-*C* phase, namely Sm-C_a phase in which the direction of the molecular tilt alternates between the smectic layers [6,8]. Fig. 6.2(b) displayed the growth of irregular stripes over the texture of

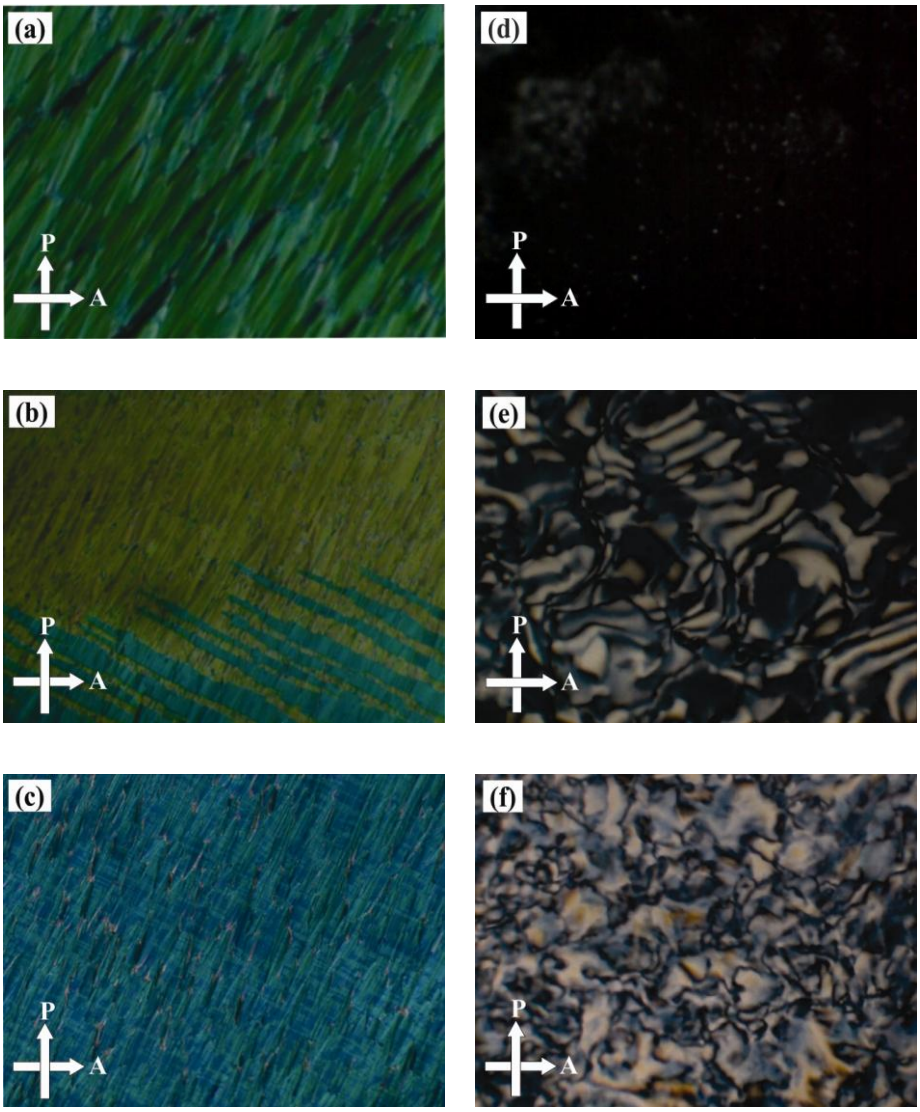

Figure 6.2. Optical texture observed for a mixture with mol fraction x_{7OCB} = 0.184 in homogeneous alignment (a-c) and homeotropic alignment (d-f). (a) Sm-*A* phase at 380 K, (b) Sm-C_s phase at 369 K, (c) Sm-C_a phase at 360 K, (d) Sm-*A* phase at 378 K, (e) Sm-C_s phase at 371 K, (f) Sm-C_a phase at 365 K. Arrows indicates the direction of the polarizers.

the Sm-C_s phase. Again in homeotropic alignment the Sm-C_a phase exhibits the schlieren texture which strongly differs from that of the Sm-C_s phase. This type of schlieren texture is accompanied by some disclination points with two brushes (S = 1/2) in addition to four brushes (S = 1). Therefore, it indicates a Sm-*C* like organization in which the layer planes are tilted with respect to the molecules and it confirms its anticlinic structure [6]. Moreover, the Schlieren

texture strongly fluctuates near the Sm-C_s–Sm-C_a transition which is a characteristic behavior at the synclinic–anticlinic transitions. The reason for such typical change in texture is due to the fact that the reorientation of the molecular tilt proceeds step by step in every second layer [32]. Interestingly, the birefringence value decreases at that transition which is also verified by the textural color change from yellow to blue in accordance with Michel Levy interference color chart [33].

6.4. Phase diagram

In this work, a rod-like compound (7OCB) was used as a dopant in the host hockey-stick-shaped compound (H-22.5). Particular focus has been taken in the region where the concentration of 7OCB is less compared to the host mesogen. Several mixtures were prepared by adding small amounts of the calamitic compound (having molar concentrations ranging between 0.05 and 0.211) into the hockey stick-shaped molecule H-22.5.

The partial phase diagram of the binary system consisting of 7OCB and H-22.5 for nine different mixtures is depicted in Fig. 6.3 which includes the *I*–Sm-*A*, Sm-*A*–Sm-C_s and Sm-C_s–Sm-C_a transitions as obtained from polarizing optical microscopy. The pure calamitic compound shows a stable *I*–*N*–Cr phase sequence as being cooled from the isotropic state. Conversely, the pure hockey stick-shaped compound comprises of a nematic phase, appearing in a quite small temperature range (~ 0.3 K) and two polymorphic tilted smectic phases, the synclinic smectic-*C* (Sm-C_s) as well as the anticlinic smectic-*C* (Sm-C_a) phases. In the Sm-C_s phase, the direction of the molecular tilt is the same in adjacent smectic layers, whereas it alternates between the layers of the Sm-C_a phase [6,8].

The addition of calamitic molecules imparts a dramatic influence on the phase behavior of the mixtures involving angular mesogenic host. Although, the hockey stick-shaped host H-22.5 possesses a small nematic temperature

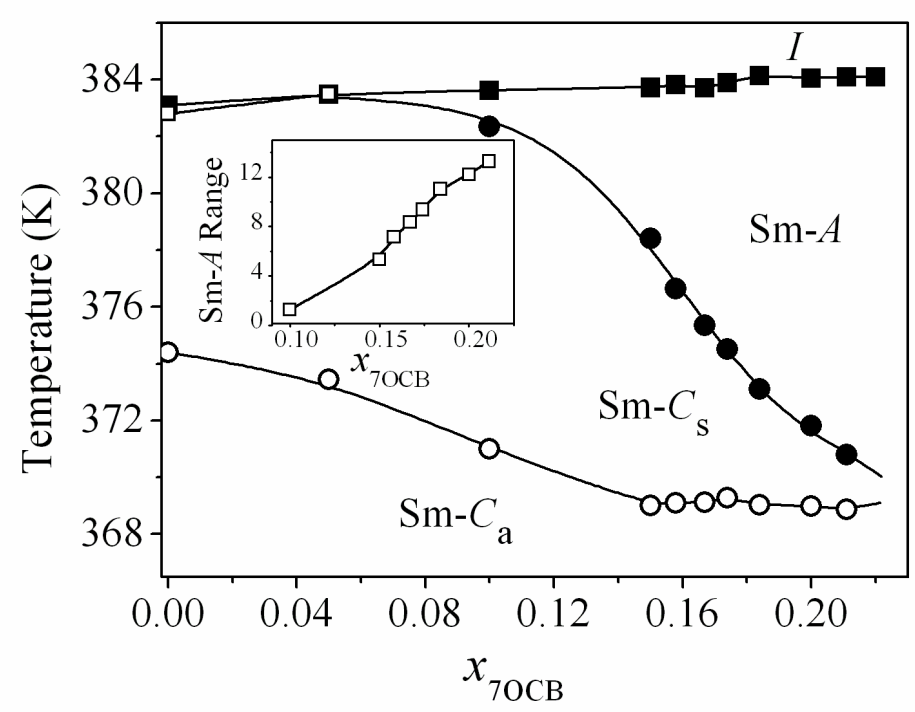

Figure 6.3. Partial phase diagram of the binary system comprising of 7OCB and H-22.5. x_{7OCB} denotes the mole fraction of 7OCB. *I* – isotropic phase, Sm-*A* – smectic-*A* phase, Sm-C_s – smectic-C_s phase, Sm-C_a – smectic-C_a phase □: *N*–Sm-C_S phase transition; ■: *I*–Sm-*A* phase transition; ●: Sm-*A*–Sm-C_S phase transition; ○: Sm-C_s–Sm-C_a phase transition temperatures. The inset shows the concentration dependence of the Sm-*A* range for the present system. Solid lines are drawn for guidance to the eye.

range, introduction of a small quantity of the nematogenic rod-like compound initially decreases the width of the nematic phase. Further increasing the quantity of the rod-like mesogenic molecules leads to completely destabilization of the nematic phase of the host compound and gives rise to an induction of Sm-*A* phase in certain molar concentration range of the binary system. Therefore, the presence of hockey-stick-shaped molecule plays a decisive role for induction of Sm-*A* phase of the studied mixtures at the Sm-*A*–Sm-*C* transition. Moreover, the Sm-*A* width increases further with the increase in the molar concentration of 7OCB, resulting a sharp reduction of Sm-C_s phase range of the bent mesogenic compound. This may be due to the fact that the addition of 7OCB in the angular mesogenic medium (H-22.5) weaken the coupling between the smectic-*A* (Ψ) and smectic-*C* (θ) order parameters and

corresponding sharp enhancement of the Sm-*A* width finally eliminates both the Sm-C_s and Sm-C_a phases. In the present binary system, both the Sm-C_s and Sm-C_a phases are found to disappear for the mixtures having molar concentration $x_{7OCB} > 0.211$ and only the Sm-*A* phase predominantly appears in the phase diagram. The variation of the Sm-*A* phase range against the molar concentrations has also been presented in the inset of Fig. 6.3. However, an augmentation of the Sm-*A* temperature range has been observed from a value 1.2 K to 13.5 K.

6.5. Optical birefringence measurements

The optical birefringence (Δn) measurement was carried out by high-resolution optical transmission [34-37] as well as thin prism techniques [38] for all of the binary mixtures. Fig. 6.4(a-b) illustrates the temperature dependence of optical birefringence data for the two representative mixtures $x_{7OCB} = 0.184$ and 0.167 obtained from both the methods, measured at a wavelength of $\lambda = 532$ nm. Such a dual measuring process enables one to get a rather precise description of Δn within the mesophases. As expected, upon cooling from the isotropic phase, a significant increase of the birefringence (obtained from both the measurement techniques) has been observed within the Sm-*A* phase. This is due to the rapid increase of short-range positional ordering via a significant growth of the cybotactic clusters from the disordered fluid state and their alignment by strong surface anchoring, which in turn facilitates in the rapid growth of the optical anisotropy of the media. On further cooling, well within the Sm-*A* phase, the Δn value increases and attains a maximum saturation value. All the studied mixtures follow the almost identical pattern. Such a change is in effect due to the enhancement of molecular ordering to a certain level in the mesogenic medium. Moreover, on entering the low-temperature Sm-C_s phase, a further sharp augmentation in birefringence value has also been observed at the Sm-*A*–Sm-C_s phase transition, which again is caused due to enhancement of the positional ordering in the tilted phase. This can be

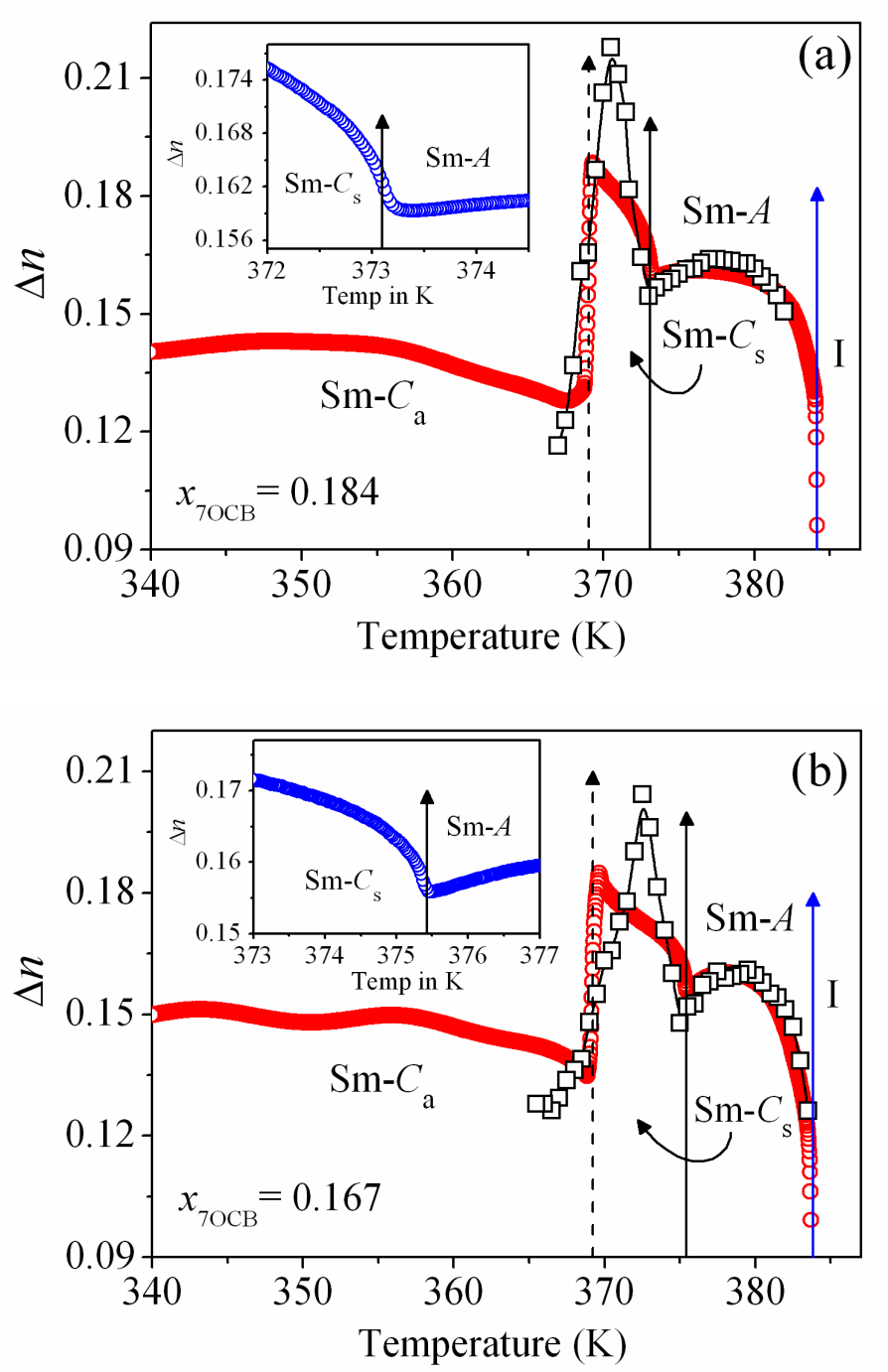

Figure 6.4. Temperature dependence of birefringence (Δn) data for (a) x_{7OCB} = 0.184 and (b) x_{7OCB} = 0.167. ○: Birefringence data from optical transmission method, □: Birefringence data from thin prism technique. Blue solid arrows indicate isotropic to smectic-*A* (*I*–Sm-*A*) phase transition temperatures (T_{IA}), black solid arrows indicate the smectic-*A* to smectic-*C* (Sm-*A*–Sm-C_s) phase transition temperatures (T_{AC}) and dashed arrows indicate the smectic-C_s to smectic-C_a phase transition temperatures (T_{CC}). Insets show the variation of birefringence in the vicinity of Sm-*A*–Sm-C_s transition temperature (T_{AC}).

explained due to the fact that the molecular long axes in the Sm-C_s phase of the surface aligned planar cell (of thickness 7.7 μm bulk sample) are oriented parallel to the aligning surface and the layers are tilted with respect to the surface alignment [6]. However, the temperature variation of Δn in the Sm-C_s phase is quite rapid with respect to that in the Sm-*A* phase. Again the birefringence value sharply decreases at the Sm-C_s–Sm-C_a phase transition and remains more or less constant throughout the Sm-C_a phase for all the mixtures under study. Since the transition to the Sm-C_a phase leads to an effective reorientation of the molecules to form an anticlinic arrangement, the molecules in this phase are now tilted with respect to the surface, causes a drop in the parallel component of the polarizability, *i.e.*, along the molecular long axis, thereby reducing the polarizability anisotropy and hence the birefringence of the material. Such a lowering of birefringence has also been observed from the color change of the optical texture during the phase transition. It is evident that the sharp change of the optical birefringence at the Sm-C_s–Sm-C_a phase transition clearly indicates a first order nature of that transition. The overall profile of the birefringence data is in close agreement with the findings for the pure hockey stick-shaped compounds as well as their multi-component mixtures [6,39] and also for few other bent-shaped mesogens [40]. A quite fair conformity between the values of Δn obtained from both the methods has been found within the temperature range of the Sm-*A* phase, but they differ in the lower temperature Sm-*C* phases due to the weak surface anchoring effect of the bulk sample within the prism. However, both the sets of data clearly exhibit a significant enhancement in the vicinity of Sm-*A*–Sm-C_s phase transition along with a sharp decrease at the Sm-C_s–Sm-C_a phase transition.

6.6. Critical behavior at the Sm-*A*–Sm-*C* phase transition

The high-resolution optical birefringence data has been used to obtain an insight into the critical behavior at the Sm-*A*–Sm-C_s phase transition. Following

the same procedure as discussed in chapter 5, the present system is also deals with the critical fluctuation in the vicinity of the transition point by investigating the precise Δn data. As the optical birefringence data exhibit no significant discontinuity at the Sm-*A*–Sm-*C* phase transition, a differential quotient Q(T) has been introduced with the following form [41,42]

$$\mathrm{Q}(T) = -\frac{\Delta n(T) - \Delta n(T_{AC})}{T - T_{AC}} \tag{6.1}$$

where $\Delta n(T_{AC})$ is the birefringence value at the Sm-*A*–Sm-*C* transition temperature (T_{AC}) and this temperature was obtained by locating the minimum value of temperature derivative of Δn at that transition. The temperature-dependent variation of Q(T) for all of the mixtures is represented in Fig. 6.5. All of the Q(T) data exhibit a noticeable divergent character on both sides of the transition temperature and demonstrate an asymmetry between the Q(T) wings in the Sm-*A* and Sm-*C* phases. Moreover, the peak height of Q(T) monotonically decreases as the concentration of rod-like compound increases. In an attempt to describe the limiting behavior of the quotient Q(T) at that transition, the following renormalization group expression including the first order corrections-to-scaling term has been used to fit the experimental data [42,43].

$$\mathrm{Q}(T) = \frac{A^{\pm}}{\alpha'}|\tau|^{-\alpha'}(1 + D^{\pm}|\tau|^{\Delta}) + E(T - T_{AC}) + B^{\pm} \tag{6.2}$$

where $\tau = (T - T_{AC})/T_{AC}$, ± denote terms above and below $T_{AC,}$ $A^{\pm}$ denotes the critical amplitudes, $D^{\pm}$ are the coefficients of the first corrections-to-scaling terms, α' is the critical exponent similar to specific heat capacity critical exponent α, Δ is the first corrections-to-scaling exponent and $B^{\pm}$ presents the constant combined critical and regular background term while $E(T\text{-}T_{NA})$ corresponds to a temperature-dependent part of the regular background contribution. Moreover, the value of Δ is kept fixed at a value 0.5 without any further variation. The values of the parameters as extracted from the fit process are tabulated in Table 6.1, while the corresponding fits are presented as solid

lines in Fig. 6.5 at a reduced temperature range $|\tau|_{max} = 4\times10^{-3}$. In the region above and below the Sm-*A*–Sm-C_s transition, fits have also been carried out for two other reduced temperature ranges of $|\tau|_{max} = 2\times10^{-3}$ and 6×10^{-3}. Corresponding best-fit parameter values are also summarized in the Table 6.1.

It is quite evident that the temperature dependence of Q(*T*) for all the binary mixtures close to T_{AC} have been well described by Eq. (6.2), suggesting a good agreement between the experimental optical birefringence data and the theoretical power-law behavior considered here. The quality of the fits have been tested with the aid of the reduced error function χ_v^2 [44,45], ranging between 1.01 to 1.44 which represents a good fit to the model expression

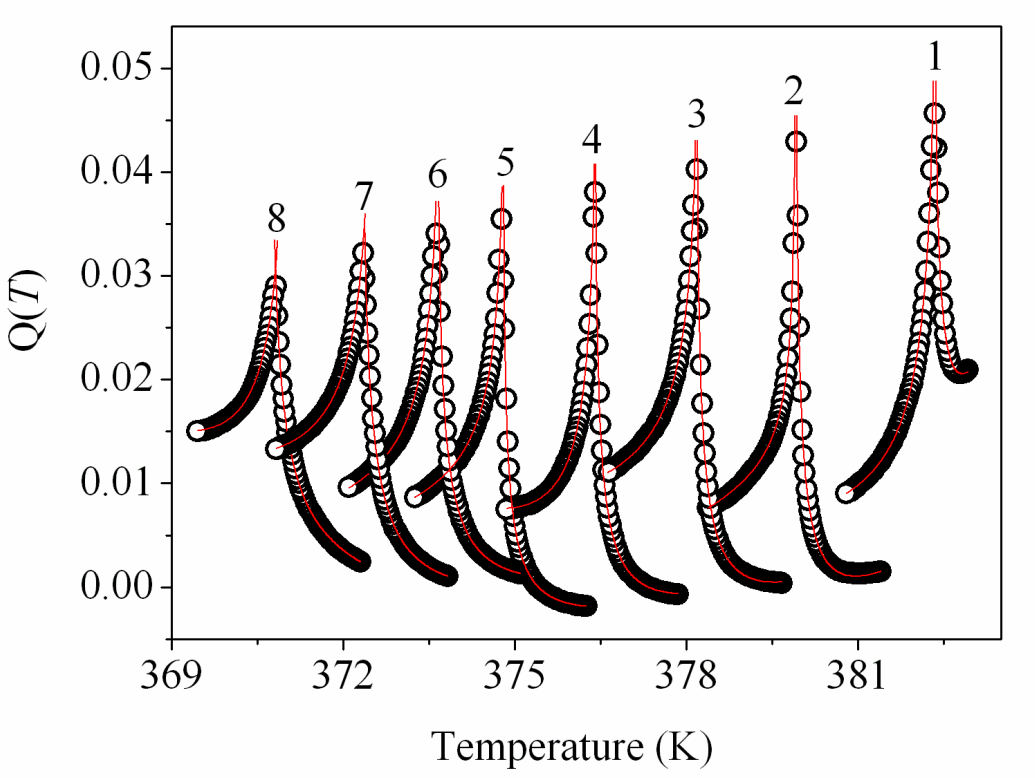

Figure 6.5. The temperature dependence of Q(*T*) in the vicinity of Sm-*A*–Sm-C_s transition in mixtures of H-22.5 and 7OCB for $|\tau|_{max} = 4\times10^{-3}$. 8: x_{7OCB} = 0.211; 7: x_{7OCB} = 0.2; 6: x_{7OCB} = 0.184; 5: x_{7OCB} = 0.174; 4: x_{7OCB} = 0.167; 3: x_{7OCB} = 0.158; 2: x_{7OCB} = 0.15; 1: x_{7OCB} = 0.1. All of these Q(*T*) data have been shifted in temperature axis for the guidance of eye as follows: curve 7 by +0.5 K, curve 6 by +0.5 K, curve 4 by +1 K, curve 3 by +1.5 K, curve 2 by +1.5 K. Solid lines representing the fits to Eq. (6.2).

Table 6.1. Results corresponding to the best fit for Q(*T*) near Sm-*A*–Sm-*C* phase transition obtained in accordance with Eq. (6.2) and related χ_v^2 values associated with the fits. $|\tau|_{\max}$ presents the upper limit of reduced temperature considered for these fits.

x_{7OCB}	$\|\tau\|_{max}$	α'	A^-/A^+	D^-/D^+	χ_v^2
0.211	0.006	0.399±0.013	1.292±0.012	1.001±0.020	1.35
	0.004	0.394±0.006	1.292±0.041	0.999±0.054	1.13
	0.002	0.399±0.013	1.428±0.634	1.010±0.445	1.12
0.200	0.006	0.437±0.013	1.328±0.027	1.000±0.082	1.13
	0.004	0.437±0.009	1.328±0.062	1.000±0.042	1.16
	0.002	0.443±0.019	1.327±0.591	0.999±0.399	1.15
0.184	0.006	0.487±0.004	1.379±0.084	1.002±0.050	1.08
	0.004	0.488±0.007	1.379±0.101	1.004±0.075	1.38
	0.002	0.483±0.025	1.250±0.431	1.004±0.302	1.29
0.174	0.006	0.501±0.010	1.579±0.098	0.994±0.050	1.06
	0.004	0.501±0.006	1.579±0.071	1.009±0.084	1.03
	0.002	0.501±0.008	1.500±0.213	0.984±0.111	1.13
0.167	0.006	0.501±0.003	1.522±0.069	1.001±0.040	1.21
	0.004	0.499±0.011	1.591±0.068	0.995±0.039	1.44
	0.002	0.504±0.018	1.579±0.492	0.984±0.222	1.23
0.158	0.006	0.502±0.004	1.440±0.070	0.999±0.058	1.17
	0.004	0.501±0.006	1.440±0.081	0.999±0.074	1.10
	0.002	0.498±0.022	1.591±0.555	0.998±0.281	1.18
0.15	0.006	0.500±0.007	1.583±0.086	1.007±0.037	1.42
	0.004	0.499±0.018	1.577±0.046	1.012±0.023	1.37
	0.002	0.503±0.029	1.650±0.757	1.011±0.157	1.32
0.1	0.006	0.501±0.012	1.571±0.091	1.001±0.044	1.36
	0.004	0.500±0.012	1.571±0.108	1.015±0.078	1.01
	0.002	0.499±0.018	1.591±0.639	1.024±0.171	1.17

considered. Moreover, in each of the mixtures, the critical exponent α' values are found to be practically constant for all of the three fit ranges. However, among the three fit ranges, the fitted curve over the reduced temperature range

$|\tau|_{max}$ = 4×10^{-3} has found to be quite satisfactory with the experimental data throughout the analysis for the Sm-*A*–Sm-*C* transition.

In the present investigated system, the effective critical exponent α' assumes a value almost equal to 0.5 for the mixture concentration x_{7OCB} = 0.1, 0.15, 0.158, 0.167 and 0.174, indicating non-classical tricritical behavior of the Sm-*A*–Sm-*C* phase transition. Despite the sharp change of the transition temperatures with the mixing ratio, no feature of the Fisher renormalization [46] of the critical exponent has been observed in these mixtures. With increasing the concentration of 7OCB, the values of α' monotonically decreases from the tricritical value 0.501 ± 0.006 for the mixture x_{7OCB} = 0.174 to 0.394 ± 0.006 for the mixture x_{7OCB} = 0.211. Therefore, the coupling between the smectic-*A* (Ψ) and smectic-*C* (θ) order parameter becomes considerably weaker for a relatively small increase in the concentration of the calamitic nematogen within the mixtures. Such an outcome is possibly due to the modification in effective intermolecular interaction and the local molecular ordering in the host medium, which drives the transition from first order to second order character. Thus, the non-universal values have been obtained for the effective critical exponent α' and hence indicating a crossover character for the Sm-*A*–Sm-*C* phase transitions in the present investigated binary system. The variation of extracted critical exponent values with the temperature ratio (T_{NA}/T_{IN}) is illustrated in Fig. 6.6 (a). An extrapolation of a quadratic fit to the α' values results a crossover from second order to first order for a composition x_{7OCB} = 0.179 with α' = 0.5 and the corresponding temperature ratio (*i.e.*, T_{AC}/T_{AI}) is being 0.972. This temperature ratio has been found to be almost identical with that obtained from previously discussed calamitic homologous system (*i.e.*, chapter 5) in the vicinity of Sm-*A*–Sm-*C* phase transition [31]. Moreover, the observed quotient A^-/A^+ reveals a value nearly equal to 1.6 for the tricritical compositions which fairly agrees with the theoretical prediction for the tricritical appearance and for rest of the mixtures it varies between 1.250 and

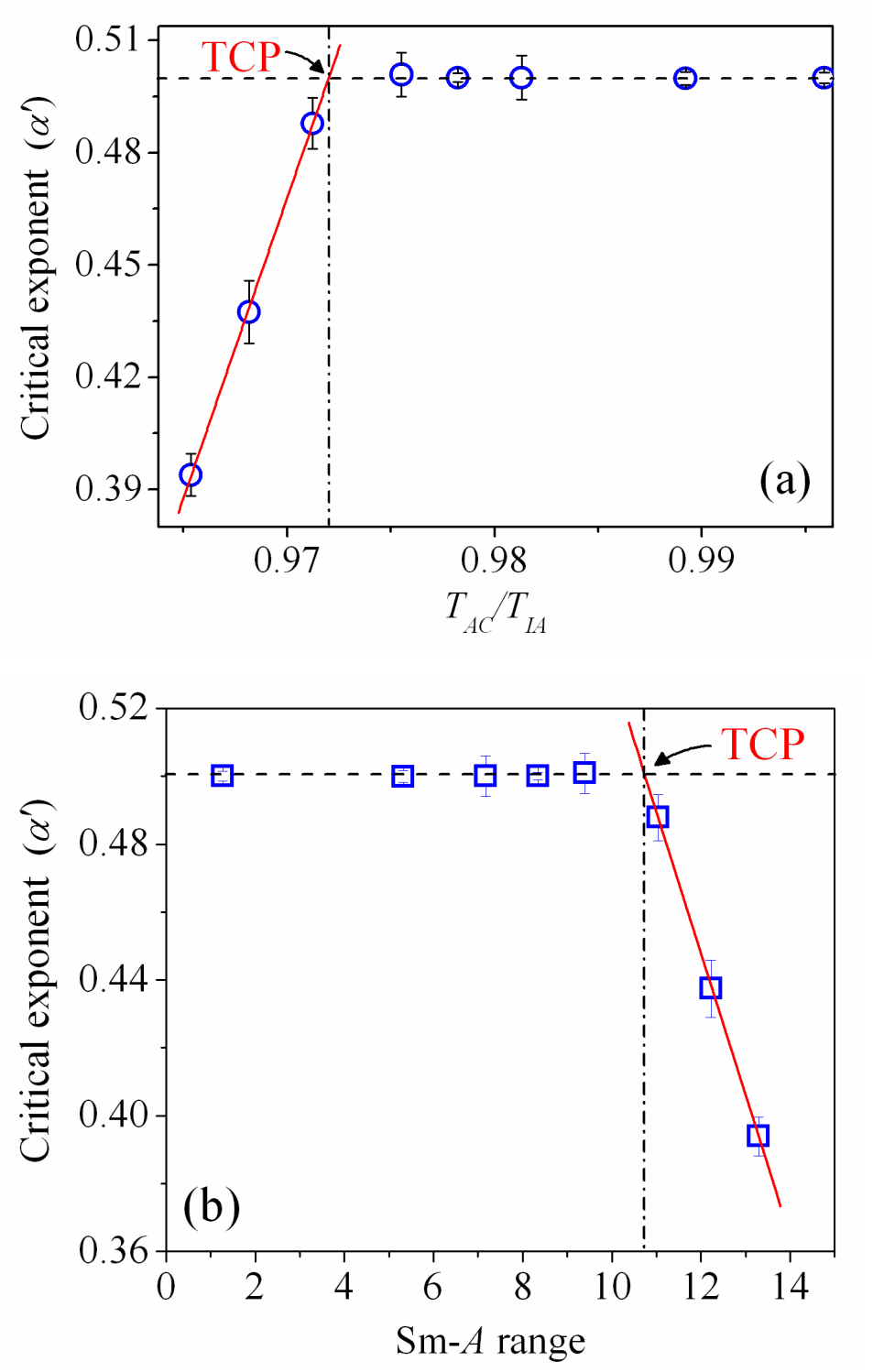

Figure 6.6. Variation of the effective critical exponent against (a) the temperature ratio T_{AC}/T_{IA} and (b) the temperature width of Sm-*A* phase at the Sm-*A*–Sm-*C* phase transition in the present investigated binary mixtures. The vertical dashed lines correspond to the tricritical point (TCP). The solid lines (red) are the 2nd order fit to the data points.

1.428. Conversely, the value of parameter ratio D^-/D^+ is nearly equal to 1 for all of the investigated mixtures, divulging a close agreement to the theoretical prediction. Additionally, a variation of effective critical exponent α' with the temperature width of the Sm-*A* phase has been explored which is depicted in Fig. 6.6(b). The present binary system indicates that the α' value lies on the tricritical limit ($\alpha' \cong 0.5$) for the five mixtures having the dopant concentration $x_{7OCB} \leq 0.174$. Accordingly, the tricritical behavior of the Sm-*A*–Sm-*C* phase transition has also been observed up to the Sm-*A* temperature range ~9.2 K and further increase of the Sm-*A* width (greater than 11 K) drives the transition to second order in nature. Therefore, the critical exponent α' demonstrates a crossover from the tricritical limit toward the *XY*-like value with increase in the Sm-*A* temperature range. An extrapolation of these extracted critical exponent values exhibit a crossover point (first order to second order in nature) for a Sm-*A* temperature range ~10.6 K, which also agrees well with the finding observed in previous chapter.

6.7. Tricritical fitting

Based on the magnitude of the effective α' values discussed in the previous section, it has been observed that the mixtures having concentration $x_{7OCB} < 0.179$ are close to or above the tricritical composition. To test the possibility of first order character of the Sm-*A*–Sm-*C* phase transition and to validate the yielded values of the critical exponent in the tricritical limit, an extensive analysis has been performed on the mixtures those are found to exhibit tricritical value of α'. The analysis has been carried out using a more general form for Q(*T*), including the first and second order correction terms which are required in describing the present data [47] and can be expressed as:

$$Q(T) = \frac{A^{\pm}}{\alpha'}|\tau|^{-\alpha'}\left(1 + D_1^{\pm}|\tau|^{\Delta_1} + D_2^{\pm}|\tau|^{2\Delta_1}\right) + E(T - T_{AC}) + B^{\pm} \quad (6.3)$$

where D_2 is the coefficients of the second corrections-to-scaling terms and other parameters are same as said for Eq. (6.2).

In this case, Δ_1 assumes a value 0.5 and the investigation has been performed for the tricritical compositions by fixing the effective α' value at 0.5. Ema *et al.* have also shown that for the tricritical fit, Δ_1 value lies close to 0.5 [48]. As a consequence of imposing the values in Eq. (6.3), the first corrections-to-scaling term merges with B and a new constant term F is introduced. Therefore, Eq. (6.3) is now simplified to [49]:

$$\mathrm{Q}(T) = \frac{A^{\pm}}{\alpha'}|\tau|^{-1/2}\left(1 + D_2^{\pm}|\tau|\right) + E(T - T_{AC}) + F^{\pm} \qquad (6.4)$$

Moreover, the stability of the fits to Eq. (6.4) has also been tested over three different ranges of reduced temperature: range-**A** ($|\tau|_{max}$ = 2×10^{-3}), range-**B** ($|\tau|_{max}$ = 4×10^{-3}) and range-**C** ($|\tau|_{max}$ = 6×10^{-3}). Corresponding fits to the experimental data with Eq. (6.4) have been illustrated by the solid lines for all the compositions x_{7OCB} < 0.179 in Fig. 6.7(a-b) for range-**B** and range-**A** respectively, while the fitted parameters are tabulated in Table 6.2. The quality of these fits has been assessed by calculating the related reduced error function χ_v^2 value [44,45] and found to be limited within 1.08 and 1.62 and thus signifying consistent fits. In the present analysis, it has been found that the parameter $D_2^{\pm}$ emerging a negative value, suggesting a qualitative agreement with those previously obtained for the tricritical *N*–Sm-*A* phase transition [50-52]. However, the quotient D_2^-/D_2^+ has been found to be $D_2^-/D_2^+ < 1$ for the range-**A** and range-**C** as observed from Table 6.2, while the parameter D_2^- is more or less equal to its counterpart D_2^+ (*i.e.*, $D_2^- \approx D_2^+$) for the range-**B**, indicating a close agreement with the theoretical prediction $D_2^- = D_2^+$ for the *N*–Sm-*A* phase transition [49,52]. On the other hand, a small systematic variation has been observed for the quotient A^-/A^+ over the influence of dopant concentration. Additionally, the extracted values of that quotient appear in a range between 0.85 and 1.062 for the fit range-**A** and **B**, while it exhibits some higher values for the fit range-**C**. However, it is expected to be 1.6 at the tricritical point in accordance with the theoretical prediction for the *N*–Sm-*A*

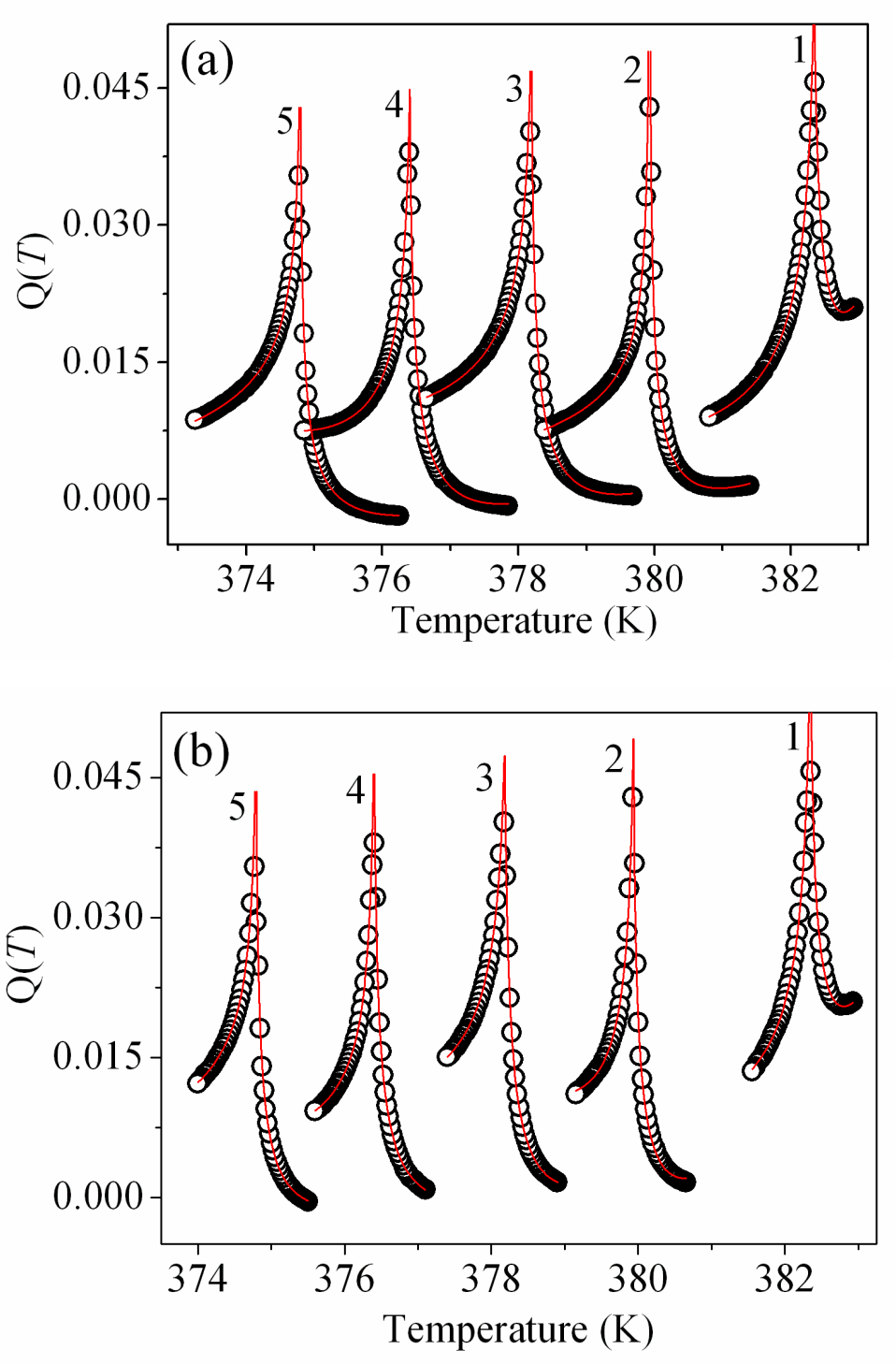

Figure 6.7. The temperature dependent variation of Q(T) in the vicinity of Sm-A–Sm-C transition in mixtures of H-22.5 and 7OCB for (a) fit range-**B** ($|\tau|_{max}$ = 4×10^{-3}), and (b) fit range-**A** ($|\tau|_{max}$ = 2×10^{-3}). 5: x_{7OCB} = 0.174; 4: x_{7OCB} = 0.167; 3: x_{7OCB} = 0.158; 2: x_{7OCB} = 0.15; 1: x_{7OCB} = 0.1. These Q(T) data has been shifted in temperature axis for the guidance of eye as follows: curve 7 by +0.5 K, curve 6 by +0.5 K, curve 4 by +1 K, curve 3 by +1.5 K, curve 2 by +1.5 K.

Table 6.2. Results corresponding to the best fit for Q(*T*) near Sm-*A*–Sm-*C* phase transition obtained in accordance with Eq. (6.4) and related χ_v^2 values associated with the fits. $|\tau|_{max}$ presents the upper limit of reduced temperature considered for these fits.

x_{7OCB}	$\|\tau\|_{max}$	10^4A^+	A^-/A^+	z	D_2^+	D_2^-/D_2^+	χ_v^2
0.174	0.006	1.7±0.024	1.353±0.019	0.59437	-165.46±1.56	0.459±0.011	1.08
	0.004	1.8±0.035	0.966±0.034	0.71839	-160.81±2.15	1.002±0.018	1.12
	0.002	2.0±0.018	1.019±0.016	0.70061	-166.50±1.04	0.429±0.020	1.10
0.167	0.006	2.1±0.038	1.347±0.024	0.59608	-166.20±1.73	0.758±0.011	1.37
	0.004	2.4±0.035	1.011±0.023	0.70278	-169.58±1.78	1.000±0.014	1.13
	0.002	2.3±0.030	1.042±0.022	0.69229	-166.99±1.47	0.462±0.009	1.32
0.158	0.006	2.2±0.036	1.344±0.022	0.59694	-167.49±1.39	0.814±0.010	1.08
	0.004	2.3±0.051	1.052±0.032	0.68832	-180.35±1.21	1.001±0.011	1.45
	0.002	2.8±0.035	1.062±0.016	0.68505	-167.35±2.89	0.500±0.013	1.25
0.15	0.006	2.3±0.014	1.348±0.008	0.5958	-177.00±1.38	0.853±0.013	1.62
	0.004	2.0±0.032	0.850±0.020	0.76194	-203.24±2.99	0.995±0.017	1.23
	0.002	2.6±0.043	0.986±0.019	0.71194	-168.00±2.70	0.500±0.021	1.45
0.1	0.006	2.5±0.074	1.320±0.039	0.60386	-179.37±2.13	0.836±0.013	1.14
	0.004	3.7±0.017	0.946±0.026	0.72645	-221.86±1.90	0.991±0.010	1.30
	0.002	3.1±0.017	0.973±0.015	0.71659	-186.53±3.70	0.499±0.015	1.12

phase transition [50-52]. Therefore, in the present system the extracted values of the quotient A^-/A^+ are non-universal over the variation of fit ranges. According to Fisher and Sarbach [53,54], this type of amplitude ratios at the tricritical point can be well described by an exactly solvable spherical (n = ∞) model, where A^-/A^+ is a function of the single variable $z = (a/R_0)^3$, and can be expressed as $A^-/A^+ = (1-z^2)^{1/2}/z$. Here a is the lattice spacing and R_0 is the range of interaction. Furthermore, while z goes to zero, the range of interaction becomes infinitely large and then A^-/A^+ approaches to infinity, recovering the Landau behavior. In the present analysis, the extracted z values are found to be very close to 0.7 for fit range-**A** and **B** (Table 6.2). Conversely, the parameter z reveals a relatively smaller value for the fit range-**C**. The representation of these z values with the variation of the amplitude ratio

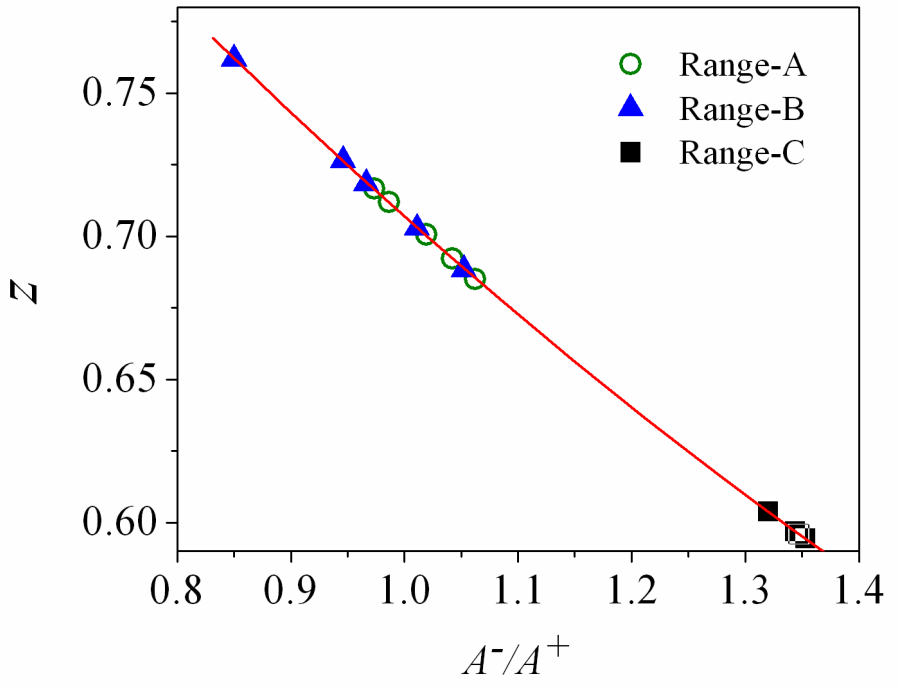

Figure 6.8. The representation of extracted *z* values with the variation of the amplitude ratio A^-/A^+ over three fit ranges in the vicinity of Sm-*A*–Sm-*C* transition. Solid line is a 2nd order polynomial to the data points.

A^-/A^+ is given in Fig. 6.8. The extracted *z* values for the smaller fit ranges in the present system reveals a well agreement with the reported values at the tricritical *N*–Sm-*A* phase transition for polar cyanobiphenyls [50], while they are found to be quite higher than the reported values of $z = 0.12$ for ^{3}He-^{4}He mixtures and $z = 0.21$ for the metamagnet $Dy_3Al_5O_{12}$ [Dysprosium Aluminum Garnet (DAG)] [53,54]. Therefore, it can be concluded that the order character of the Sm-*A*–Sm-*C* transition for the mixtures $x_{7OCB} = 0.1$, 0.15, 0.158, 0.167 and 0.174 are truely tricritical in nature. The fitting results in Table 6.2 especially over the fit range-**A** and **B** demonstrates a well-consistency with the renormalization group expression considered here, in which the first and second order correction terms plays a crucial role for the tricritical nature of the Sm-*A*–Sm-*C* phase transition. Moreover the agreement between the observed data and the fitted curve to Eq. (6.4) is quite well over the region 2×10^{-3} and 4×10^{-3}.

A qualitative comparison has been made for the values of effective critical exponent (α') in the vicinity of Sm-*A*–Sm-*C* phase transition in the present binary system with the same obtained from the homologous calamitic binary mixtures reported in previous chapter. All the values of α' extracted from both the binary systems are plotted against related temperature ratios (similar to McMillan ratio) in Fig. 6.9. For the binary system reported here, three mixtures have the temperature ratios (T_{AC}/T_{IA}) less than 0.972 and the extracted value of α' has been found to demonstrate a non-universal behavior lying in between the tricritical and 3D-*XY* limit. However, they follow the same curve as indicated by red solid line in Fig. 6.9 obtained from the study of binary mixtures consisting of the homologous rod-like compounds.

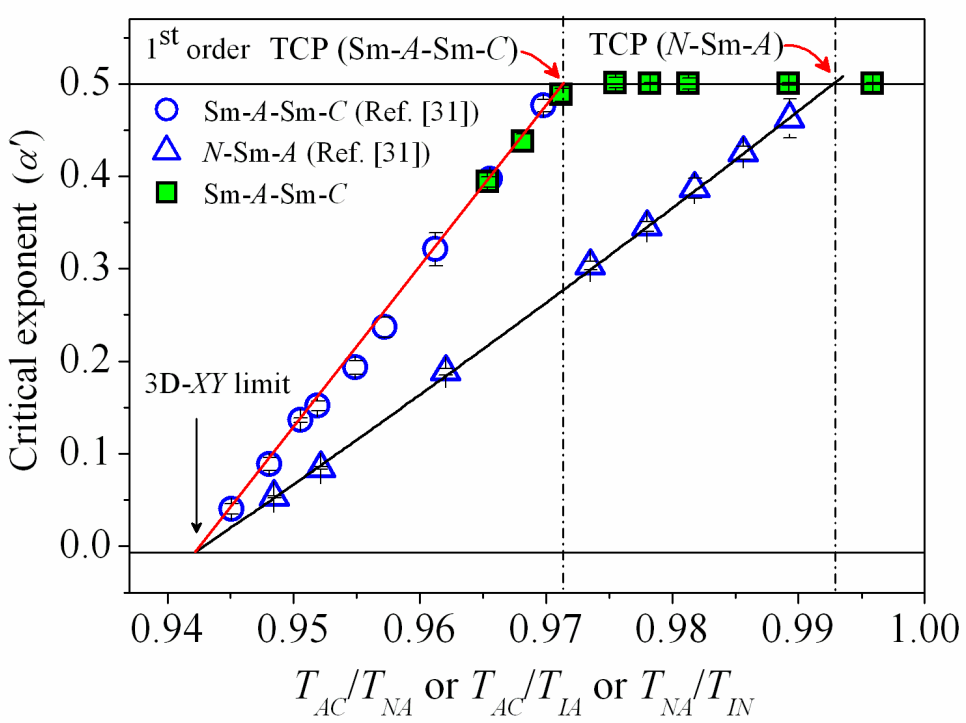

Figure 6.9. Variation of the effective critical exponent (α') with the temperature ratio T_{AC}/T_{IA} for Sm-*A*–Sm-C_s phase transitions of the present binary system. ○: Values of α' for Sm-*A*–Sm-*C* transition from chapter 5; □: Values of α' for *N*–Sm-*A* transition from chapter 5. The vertical dashed-dot lines are corresponding to the tricritical point (TCP). The solid lines (red) are the linear fit to the data points.

On the other hand, the mixtures having temperature ratio (T_{AC}/T_{IA}) greater than 0.972 exhibit the value of α' almost equal to 0.5 signifying a Gaussian tricritical nature of the Sm-*A*–Sm-*C* phase transition. Thus the observed phenomena reveal a crossover point at a temperature ratio of 0.972, which is quite low in comparison to the McMillan ratio (T_{NA}/T_{IN}) 0.994 for the *N*–Sm-*A* phase transition [31]. Additionally, in light of the tricritical nature yielded in the *N*–Sm-*A* phase transition at a nematic phase range ~2.5 K, the Sm-*A*–Sm-*C* transition emphasizes the crossover point (second order to first order) at a temperature range of Sm-*A* phase of about ~10.5 K. Conversely, the linear fit to the α' data yields a temperature ratio (T_{AC}/T_{IA} or T_{AC}/T_{NA}) of 0.942 corresponding to the 3D-*XY* point which is found to be very close to the McMillan ratio (T_{NA}/T_{IN}), for the *N*–Sm-*A* phase transition [31,52,55]. As a result, the values of α' follows two distinctly different straight lines for the Sm-*A*–Sm-*C* and *N*–Sm-*A* phase transitions with the variation of the temperature width of the Sm-*A* and *N* phases respectively [31]. Therefore, a broad tricritical region for the Sm-*A*–Sm-*C* phase transition is experimentally revealed in the present binary system.

6.8. Conclusion

In this work, a systematic study has been performed on the high-resolution temperature-dependent optical birefringence for a binary system, consisting of a methyl group substituted hockey-stick-shaped compound, 4-(3-n-decyloxy-2-methyl-phenyliminomethyl) phenyl 4-n-dodecyloxycinnamate (H-22.5) and a calamitic heptyloxy-cyanobiphenyl (7OCB). A significant destabilization of the nematic phase along with an emergence of the Sm-*A* phase is observed in the phase diagram due to the increase in the concentration of the calamitic nematogen. The birefringence data are found to be rather successful in describing the transitional anomaly at the Sm-*A*–Sm-*C* phase transition for all the investigated mixtures. The temperature dependence of birefringence data exhibits a sharp enhancement at the Sm-*A*–Sm-*C* transition.

By analyzing the temperature derivative of optical birefringence, the power-law divergence behavior has been observed in the vicinity of the Sm-*A*–Sm-*C* transition. The related effective critical exponent (α'), describing the critical fluctuations at that transition, has appeared to be non-universal in nature. The present outcomes again confirm that the width of the Sm-*A* phase range plays an important role in determining the nature of the Sm-*A*–Sm-*C* phase transition as observed in previous chapter. Interestingly, the values of α' lie in between 3D-*XY* and tricritical point (TCP) by decreasing the Sm-*A* phase range of about ~10.5 K and further decrease in Sm-*A* range the critical exponent (α') values remain in the tricritical limit ($\alpha' = 0.5$). The manifestation of such tricritical nature has also been confirmed by analyzing the experimental data in an extended procedure with the aid of modified renormalization group expression. Consequently, the present system divulges a crossover point at a temperature ratio (similar to McMillan ratio, T_{NA}/T_{IN}) of about 0.972 for the Sm-*A*–Sm-*C* phase transition. In spite of the binary system formed by divergent molecular structure, the crossover point in the present system is in a good agreement with that obtained from the binary mixtures of the homologous compounds as reported in previous chapter (chapter 5). Interestingly, the critical exponent (α') values observed in the present system suggesting a broad tricritical range for the Sm-*A*–Sm-*C* phase transition over a wide scale of temperature ratio (from 0.972 to 0.996), which is quite unusual and probably being reported for the first time.

References:

[1] S. Chandrasekhar, in *Liquid Crystals*, 2nd ed., Cambridge University Press, New York (1992).

[2] T. Niori, F. Sekine, J. Watanabe, T. Furukawa, and H. Takezoe, *J. Mater. Chem.*, **6**, 1231 (1996).

[3] R. Pratibha, N.V. Madhusudana, and B.K. Sadashiva, *Science*, **288**, 2184 (2000).

[4] G. Pelzl, S. Diele, and W. Weissflog, *Adv. Mater.*, **11**, 707 (1999).

[5] A. Chakraborty, M.K. Das, B. Das, A. Lehmann, and C. Tschierske, *Soft Matter*, **9**, 4273 (2013).

[6] B. Das, S. Grande, W. Weissflog, A. Eremin, M.W. Schröder, G. Pelzl, S. Diele, and H. Kresse, *Liq. Cryst*., **30**, 529 (2003).

[7] G. Sarkar, B. Das, M.K. Das, U. Baumeister, and W. Weissflog, *Mol. Cryst. Liq. Cryst.*, **540**, 188 (2011).

[8] A. Chakraborty, B. Das, M.K. Das, S. Findeisen-Tandel, M.-G. Tamba, U. Baumeister, H. Kresse, and W. Weissflog, *Liq. Cryst.*, **38**, 1085 (2011).

[9] X.F. Han, S.T. Wang, A. Cady, Z.Q. Liu, S. Findeisen, W. Weissflog, and C.C. Huang, *Phys. Rev. E*, **68**, 060701 (2003).

[10] A. Chakraborty, M.K. Das, B. Das, U. Baumeister, and W. Weissflog, *J. Mater. Chem. C*, **1**, 7418 (2013).

[11] T. Otani, F. Araoka, K. Ishikawa, and H. Takezoe, *J. Am. Chem. Soc.*, **131**, 12368 (2009).

[12] C. Zhu, D. Chen, Y. Shen, C.D. Jones, M.A. Glaser, J.E. Maclennan, and N.A. Clark, *Phys. Rev. E*, **81**, 011704 (2010).

[13] Y. Takanishi, Y. Ohtsuka, Y. Takahashi, and A. Iida, *Phys. Rev. E*, **81**, 011701 (2010).

[14] R. Pratibha, N.V. Madhusudana, and B.K. Sadashiva, *Phys. Rev.* E, **71**, 011701 (2005).

[15] C.A. Shantz, and D.L. Johnson, *Phys. Rev. A*, **17,** 1504 (1978).

[16] C.C. Huang, and J.M. Viner, *Phys. Rev. A*, **25,** 3385 (1982).

[17] R.J. Birgeneau, C.W. Garland, A.R. Kortan, J.D. Litster, M. Meichle, B.M. Ocko, C. Rosenblatt, L.J. Yu, and J. Goodby, *Phys. Rev. A*, **27**, 1251 (1983).

[18] M. Meichle, and C.W. Garland, *Phys. Rev. A*, **27**, 2624 (1983).

[19] S.C. Lien, C.C. Huang, T. Carlsson, I. Dahl, and S.T. Lagerwall, *Mol. Cryst. Liq. Cryst.*, **108**, 149 (1984).

[20] S. Dumrongrattana, C.C. Huang, G. Nounesis, S.C. Lien, and J.M. Viner, *Phys. Rev. A*, **34**, 5010 (1986).

[21] P. Das, K. Ema, and C.W. Garland, *Liq. Cryst.*, **4**, 205 (1989).

[22] H.Y. Liu, C.C. Huang, Ch. Bahr, and G. Heppke, *Phys. Rev. Lett.*, **61**, 345 (1988).

[23] T. Chan, Ch. Bahr, G. Heppke, and C.W. Garland, *Liq. Cryst.*, **13**, 667 (1993).

[24] K. Ema, J. Watanabe, A. Takagi, and H. Yao, *Phys. Rev. E*, **52**, 1216 (1995).

[25] L. Reed, T. Stoebe, and C.C. Huang, *Phys. Rev. E*, **52**, R2157 (1995).

[26] K. Ema, A. Takagi, and H. Yao, *Phys. Rev. E*, **53**, R3036 (1996).

[27] K. Ema, M. Ogawa, A. Takagi, and H. Yao, *Phys. Rev. E*, **54**, R25 (1996).

[28] K. Ema, H. Yao, A. Fukuda, Y. Takanishi, and H. Takezoe, *Phys. Rev. E*, **54**, 4450 (1996).

[29] K. Ema, and H. Yao, *Phys. Rev. E*, **57**, 6677 (1998).

[30] A. Chakraborty, S. Chakraborty, and M.K. Das, *Physica B*, **479**, 90 (2015).

[31] M.K. Das, S. Chakraborty, R. Dabrowski, and M. Czerwinski, *Phys. Rev. E*, **95**, 012705 (2017).

[32] R. Stannarius, J. Li, and W. Weissflog, *Phys. Rev. Lett.*, **90**, 025502-1–4 (2003).

[33] https://applications.zeiss.com/C125792900358A3F/0/E037A9841E664961C1257906004802D6/$FILE/70_2_0110_e_michel_levy.pdf

[34] A. Saipa, and F. Giesselmann, *Liq. Cryst.*, **29**, 347 (2002).

[35] G. Sarkar, M.K. Das, R. Paul, B. Das, and W. Weissflog, *Phase Transit.*, **82**, 433 (2009).

[36] T. Scharf, in *Polarized Light in Liquid Crystals and Polymers*, Wiley, Hoboken, NJ, (2007).

[37] A. Prasad, and M.K. Das, *J. Phys.: Condens. Matter*, **22**, 195106 (2010).

[38] A. Prasad, and M.K. Das, *Phase Transit.*, **83**, 1072 (2010).

[39] A. Chakraborty, S. Chakraborty, M.K. Das, and W. Weissflog, *J. Mol. Liq.*, **265**, 536 (2018).

[40] J.A. Olivares, S. Stojadinovic, T. Dingemans, S. Sprunt, and A. Jákli, *Phys. Rev. E*, **68**, 041704 (2003).

[41] M.C. Çetinkaya, S. Yildiz, H. Özbek, P. Losada-Pérez, J. Leys, and J. Thoen, *Phys. Rev. E*, **88**, 042502 (2013).

[42] S. Erkan, M. Cetinkaya, S. Yildiz, and H. Ozbek, *Phys. Rev. E*, **86**, 041705 (2012).

[43] C.W. Garland, in *Liquid Crystals: Experimental Study of Physical Properties and Phase Transitions*, edited by S. Kumar, Cambridge University Press, Cambridge (2001).

[44] P.R. Bevington, and D.K. Robinson, in *Data Reduction and Error Analysis for the Physical Sciences*, 3rd ed., McGraw-Hill, New York (2003).

[45] A. Żywociński, and J. Phys. *Chem. B*, **107**, 9491 (2003).

[46] M. E. Fisher, *Phys. Rev.*, **176**, 257 (1968).

[47] A. Aharony, and M.E. Fisher, *Phys. Rev.B*, **27**, 4394 (1983).

[48] K. Ema, A. Takagi, and H. Yao, *Phys. Rev. E*, **55**, 508 (1997).

[49] K. Ema, A. Takagi, and H. Yao, *Phys. Rev. E*, **53**, R3036 (1996).

[50] K. Stine, and C.W. Garland, *Phys. Rev. A*, **39**, 3148 (1989).

[51] G. Nounesis, C.W. Garland, and R. Shashidhar, *Phys. Rev. A*, **43**, 1849 (1991).

[52] A. Chakraborty, S. Chakraborty, and M.K. Das, *Phys. Rev. E*, **91**, 032503 (2015).

[53] M. E. Fisher, and S. Sarbach, *Phys. Rev. Lett.*, **41**, 1127 (1978).

[54] S. Sarbach, and M. E. Fisher, *Phys. Rev. B*, **20**, 2797 (1979).

[55] S. Chakraborty, A. Chakraborty, and M.K. Das, *J. Mol. Liq.*, **219**, 608 (2016).